ISTITUTO PER I PROCESSI CHIMICO-FISICI
Laboratorio per l'Irraggiamento con Laser Intensi
Area della Ricerca CNR, Via Moruzzi, 1 56124 Pisa, Italy
e-mail la.gizzi@ipcf.cnr.it

IPCF Rapporto Interno N. 1/2008

LASER-ACCELERATED PROTON YIELD CONTROL VIA REAR-SURFACE TARGET COATING

Abstract. Laser-driven acceleration of protons up to energies of 3.5 MeV and with a beam half-angle divergence of 10° has been observed by irradiating multi-layer targets of different thickness and material with 70 fs, 600 mJ, Ti:Sa laser pulses. The experimental results suggest that target rear-surface coating with hydrogen rich material may significantly enhance the accelerated proton yield and collimation. The observations are in a qualitative agreement with the numerical results obtained with a Particle-In-Cell (PIC) code.

LASER-ACCELERATED PROTON YIELD CONTROL VIA REAR-SURFACE TARGET COATING

Sergio BETTI,* Carlo A. CECCHETTI,† Andrea GAMUCCI,‡ Antonio GIULIETTI,‡ Danilo GIULIETTI,§ Petra KOESTER,‡ Luca LABATE,‡ Tadzio LEVATO,‡ and Leonida A. GIZZI¶
Intense Laser Irradiation Laboratory, IPCF, Area della ricerca CNR, Via G. Moruzzi, 1 - Pisa, Italy

Flavio ZAMPONI, Andrea LÜBCKE, Tino KÄMPFER, Ingo USCHMANN, and Eckhart FÖRSTER
Institute for Optics and Quantum Electronics - Friedrich-Schiller-University,Max-Wien-Platz 1, 07743 Jena, Germany
(Dated: January 11, 2008)

Laser-driven acceleration of protons up to energies of 3.5 MeV and with a beam half-angle divergence of 10° has been observed by irradiating multi-layer targets of different thickness and material with 70 fs, 600 mJ Ti:Sa laser pulses. The experimental results suggest that target rear-surface coating with hydrogen rich material may significantly increase the accelerated proton yield and collimation. The observations are in a qualitative agreement with the numerical results obtained with a Particle-In-Cell (PIC) code.

I. INTRODUCTION

The advent of the Chirped Pulsed Amplification (CPA) technique[1] started a new era in the experimental investigation of laser-matter interactions by giving the opportunity of generating sub-picosecond pulses of hundreds of joules. Once focused, such pulses allow irradiation intensities above 10^{21} W/cm^2 to be reached. Consequently, a wide variety of unprecendented physical phenomena can be observed. Among these phenomena, laser-driven ion acceleration is attracting a great interest[2–12]. In fact, it is now established that bunches of heavy, positively charged particles of high energy ($\gg 1$ MeV) can be generated via laser irradiation of thin foils.

The recent growth of the attention of the scientific community towards this topic reflects the extremely diversified, relevant applications in which high energy ion beams can play a significant role, among which hadron theraphy[13–21], Inertial Confinement Fusion (ICF)[22,23] and proton imaging[24–27] are worth mentioning. In this context, laser-driven ion acceleration is a promising opportunity, in particular because of the extremely low emittance (< 0.004 mm rad) and the small half-angle divergence ($\approx 10°$), together with the high values of the currents (> 1 kA) typically characterizing such laser-accelerated beams[28,29].

Moreover, the idea of a laser-based ion accelerator is extremely interesting because of the significantly smaller environmental and economical impact of a laser driven acceleration with respect to conventional particle accelerators.

In the typical setup of an ion-acceleration-oriented experiment the laser pulse is focused onto a metallic or plastic film, i.e. on a one-layer target, and this results in the acceleration of both the foil ions and protons originating from hydrocarbon contaminants which - if not properly removed - are always present on both target surfaces[30].

Today, both experiments and numerical simulations agree on the mechanism of ion acceleration which is expected to take place in the case of tens of μm foils, which is referred to as TNSA (Target Normal Sheath Acceleration)[31–35]. In particular, such mechanism predicts that the protons are preferentially accelerated due to their more favourable charge-to-mass ratio compared to other ion species. These studies also show that the most energetic particles are accelerated from the rear side - i.e. non-irradiated side - of the target and that massive production high energy protons with one-layer, tens-of-μm targets is predominantly achieved when high intensity, picosecond-scale laser pulses are used. These conditions can only be achieved at large scale laser facilities where multi-tens of Joule laser pulses are available. On the other hand, basic acceleration can be studied even at much shorter pulse duration, achievable with much smaller (table-top) laser systems.

We performed an experiment in which a multi-TW laser system was used to study laser interaction with foil targets and to investigate charged particle acceleration. In that experiment a detailed characterization of electron acceleration was carried out and a preliminary description is given elsewhere[36]. Here we report on the production of energetic (MeV) protons with multi-layer targets of different material, with and without rear-side coating. Our study, while confirming experimental results on proton acceleration obtained in similar configurations, also shows that hydrocarbon based target rear-coating can enhance performance of laser-driven proton acceleration.

This paper is organized as follows. In Sec. II we describe the experimental setup used. In Sec. III we present the results obtained, which are subsequently discussed in Sec. IV, where results obtained with a numerical PIC code are also presented. Finally, conclusions of our study are given in Sec. V.

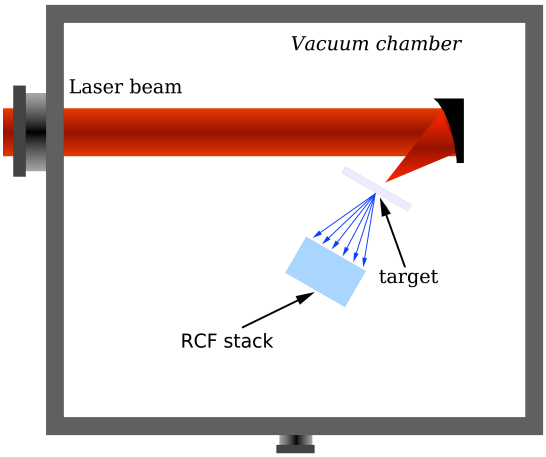

FIG. 1: Schematic layout of the experimental setup showing the laser beam, the target position and the Radiochromic film stack behind the target.

II. DESCRIPTION OF THE EXPERIMENTAL SETUP

A schematic layout of the experimental setup is presented in Figure 1. The experiment was performed at the IOQ-Jena facility using the Ti:Sa, 10 Hz, JETI laser capable of delivering up to 600 mJ in 70 fs pulses. An $f/1.2$ off-axis parabola with an angle of incidence of 45° was employed to focus the laser pulses down to 5 μm^2 focal spot, thus allowing an intensity of 5×10^{19} W/cm^2 to be achieved, corresponding to a normalized vector potential $a_0 = eA_L/m_e c^2 \approx 4.8$, e and m_e being the electron charge and mass, respectively, A_L the laser vector potential, and c the speed of light.

TABLE I: Slab composition (first column) and compound eventually used to assembly the sandwich or deposited on the target rear side (i.e. non-irradiated) surface (second column) in the shots which are relevant for the analysis presented in the present work.

Target composition[a]	Compound
(a) 5 μm Ti	none
(b) 10 μm Fe + 1.5 μm Mylar + 10 μm Ti	lacquer
(b') 10 μm Cu + 1.3 μm TiO_2 + 10 μm Fe	no-lacquer
(c) 10 μm Fe	lacquer[b]

[a]The target side which is laser-irradiated is the first one listed in every row.
[b]The spray was deposited on the non-irradiated side of the target (rear surface).

Targets consisting of either (coated or uncoated) single layer or sandwiches of different Z materials of total thickness ranging from 5 μm to 70 μm were used. A list of specifications of the target configurations taken into account in this work is given in Table I. We note that a commercial lacquer, a material usually characterized by a high content of C and H (e.g. R = $(CH_2)_{14}CH_3$), was used for either layer assembling or rear-surface target coating.

Particle detection was carried out using a stack of Radiochromic Films (RCF), which were shielded from electromagnetic radiation by a 20 μm thick Al foil. The RCF set was placed behind the target at a distance of 7 mm.

III. EXPERIMENTAL RESULTS

Figure 2 shows the densitometer scan of the first three films of the RCF stack, after irradiation of the case (a) target. According to this figure, the signal generated by charged particles impinging on the detector consists of a main filament-like pattern superimposed on a much more uniform, smooth background visible on the entire exposed circular area of the RCF. The latter signal is also visible on several films deeper in the stack and could be attributed to energetic (MeV) electrons as described in[36]. In contrast, the main signal was only detected on the first three films shown here and originates from protons or ions. As for the identification of the ion type, since the RCF is only sensitive to the dose released in the active film[37], additional information is needed to distinguish between particles

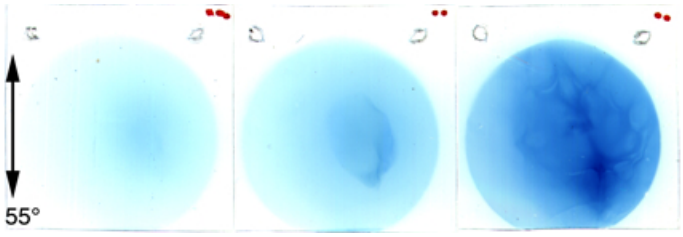

FIG. 2: Raw densitometer scan of the first three films of the RCF stack in the case of irradiation of a 5 μm thick Ti target, corresponding to case (a) in Table I.

with different charge-to-mass ratio. As we will see, particles other than electrons have been identified as protons on the basis of the modelling presented in Sec. IV.

Figure 3 shows the first RCF after irradiation of a case (b) target. The pattern obtained in this case is dramatically different from the one in Figure 2. In fact, a much more regular (circular) and uniform pattern is found with a significant reduction of the diameter if compared to the overall transverse size of the pattern of Figure 2. A uniform background due to energetic electrons similar to the one of Figure 2 is also visible in Figure 3. In contrast, measurements performed using a similar sandwich target (case b' of Table I), but assembled using standard deposition techniques, did not exhibit a detectable proton yield. In other words, these results strongly suggest that in our case, proton emission is affected by the presence of the lacquer which appears to lead to a significant increase in the proton yield.

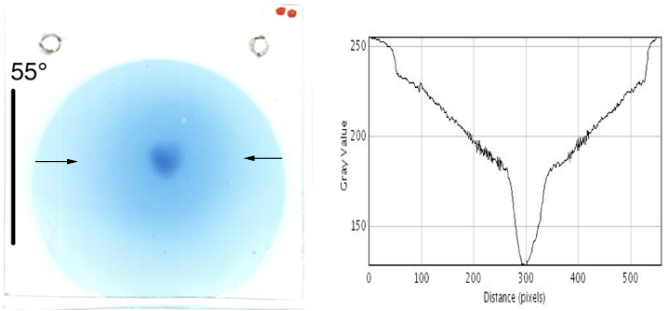

FIG. 3: Left: Raw densitometer scan of the first film of the RCF stack in the case of a 10 μm Fe + 1.5 μm Mylar + 10 μm Ti target assembled with lacquer, corresponding to case (b) in Table I. The plot on the right shows the lineout along the line indicated by the two arrows on the left image.

Following this observation, we used a target (case c) consisting of a 10 μm thick Fe film lacquer-coated on the rear side and irradiated on its clean side. Figure 4 shows the scan of the first RCF obtained in this configuration. Clearly, the pattern of the proton generated dose is much similar to the one of Figure 3. A comparison of the lineouts taken along the diameters of the patterns of Figure 3 and Figure 4 clearly shows that the proton signal in the latter case is much stronger.

The weaker proton signal observed in the case of a sandwich target can be explained by assuming that in the case of Figure 3, protons accelerated from the each layer of lacquer have to propagate through the remaining target layer(s) of Mylar and Ti. As a consequence, partial absorption of less energetic protons will occur before detection takes place, with a consequent reduction of the dose in the RCF.

In the case of Figure 4, no additional target layers are present beyond the coating layer. Therefore, no absorption occurs before protons reach the RCF stack where dose is released. These circumstances appear to be consistent with the above assumption that protons originate from the layer of lacquer used either for rear target coating or for sandwich target assembling. A quantitative analysis is in progress to further elucidate this point.

Additional enlightening information on the conditions in which proton acceleration is observed in our experimental conditions can be obtained by observing the rear-surface coating after the shot. In fact, in some cases, the coating is found to be ablated in a small circular region around the laser generated hole. A closer look to this ablated region shows that its shape resembles very closely the shape of the pattern of the proton signal on the RCF.

These details are clearly visible in the image of Figure 5 that shows the target front surface and the target rear-surface after two consecutive shots in two different positions. The front side image shows two almost identical patterns with the laser drilled hole in the centre and an annular region of approximately 2.9 mm of diameter all around. The

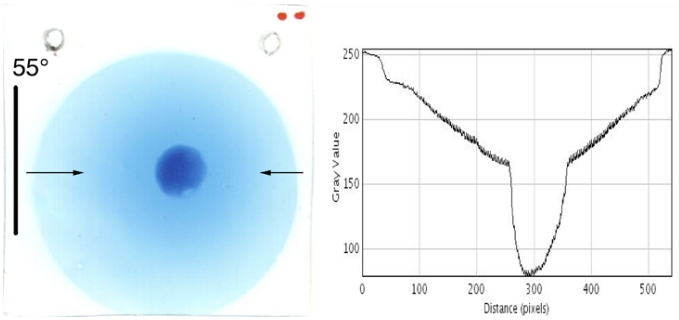

FIG. 4: Raw densitometer scan of the first RCF in the case of irradiation of a 10 μm thick Fe target coated with the lacquer on its rear surface, corresponding to case (c) in Table I. The data shown correspond to shot 1 in Fig. 5. The plot on the right shows the lineout along the line indicated by the two arrows on the left image.

coated rear-surface shows one case (upper-left on image b) in which the coating was ablated irregularly and over a much larger area than the annular region visible on the front side. Surprisingly, in the other case (lower-right), the coating was ablated in a much regular way and in a very small region. The diameter of this region is 1.9 mm, which is approximately half of the diameter of the dose released pattern of Figure 4 which was measured to be 4.3 mm. As we will discuss below, these geometrical details are consistent with a "projection" on the plane of the RCF of the ablated disk of material (ions), assuming a laminar particle beam expansion with a divergence of approximately 10°.

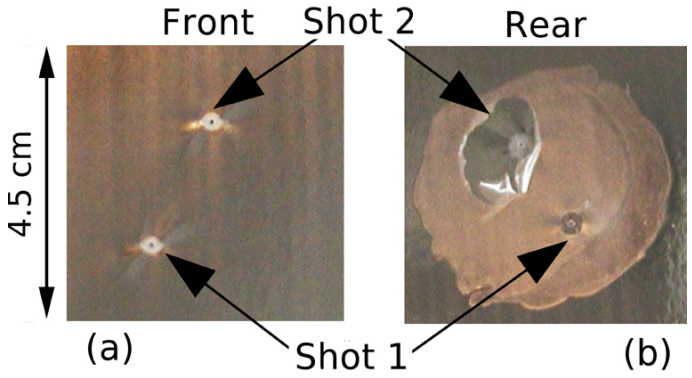

FIG. 5: Pictures of the target showing the front (irradiated) side (panel (a)) and the rear (non-irradiated) side (panel (b)) of the 10 μm thick, lacquer rear-coated Fe film after two shots.

An exciting possible conclusion of these preliminary observations is that the entire "disk" of the coating material behind the target was ablated and accelerated forward as schematically depicted in Figure 6. Clearly, our RCF based detection technique only allowed us to detect relatively energetic particles like protons, due to their higher charge-to-mass ratio. From this component we can possibly infer the dynamics of ablation of the entire disk of material. . Further investigation and additional calculations are needed to support this conclusion. In the following we describe the results of a preliminary modelling of our proton acceleration data which provides a basic identification of the main physical conditions occurring in our experiment.

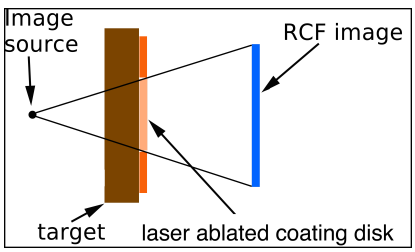

FIG. 6: Schematic layout of the geometric-optic-based procedure adopted to infer the proton beam divergence and source point after laser irradiation of a lacque rear-coated target.

IV. MORE DATA AND DISCUSSION OF THE EXPERIMENTAL RESULTS

As anticipated above, we inferred the typical proton beam emission half-angle θ by analyzing both the target rear surface shown in Figure 5 and the dose pattern on the RCF of Figure 4. In particular, we assumed the proton beam to be essentially laminar, which is a reasonable approximation due to the extremely low emittance (< 0.004 mm rad) typically characterizing laser-accelerated ions[28,29], and consequently applied the rules of geometrical optics, as schematically shown in Figure 6. We thus obtain $\theta \approx 10^\circ$, which is fully consistent with other previously published results[38]. This calculation is equivalent to assuming a virtual point-like proton source located at a distance of roughly 12 mm in front of the non-irradiated side of the target. The assumption of a virtual source is consistent with other earlier experimental observations[39].

A further characterization of the proton source has been carried out with the help of the radiographic image of the Ta grid shown in Figure 7, and has allowed us to infer the typical energy range of the protons produced in our experiment. In particular, the lower energy range $U_{\rm min}$ has been deduced by observing that the protons were transmitted through the 20 μm thick Al foil placed in front of the RCF stack. Therefore, by using the numerical code SRIM[40] we find $U_{\rm min} \approx 1.2$ MeV. The higher proton energy has been inferred by observing that, as can be clearly seen in Figure 7, the protons transmitted through the Al foil were not capable of penetrating the full diameter of a single Ta wire, which is equal to $d = 35$ μm. Therefore, according to additional calculations performed using the code SRIM, the upper value to the proton energy is found to be $U_{\rm max} \approx 3.56$ MeV.

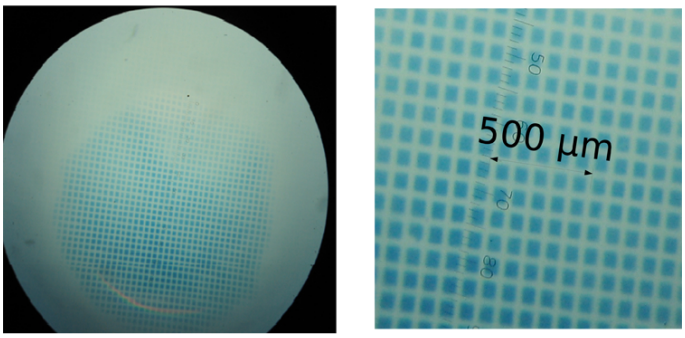

FIG. 7: Left: Raw densitometer scan of the first RCF showing the proton beam pattern after transmission through a 35 μm thick Tantalum grid with a 100 μm mesh period. The proton beam was produced by irradiation of a 10 μm thick Fe target with rear-side lacquer coating, corresponding to case (c) in Table I. The data correspond to shot 2 in Figure 5. Right: magnification of the central region of the image on the left.

In order to achieve a basic understanding of the above experimental results, we performed numerical, PIC simulations[41]. The simulations are 3D in the particles velocities and 1D in the cartesian coordinates. The target is modeled as a fully ionized, quasineutral, Ti bulk plasma. A thinner layer of fully ionized, hydrogen plasma is added on the rear side - i.e. the non-irradiated side - in order to model hydrogen rich coating.

The electron density profile, qualitatively sketched in Figure 8, ramps up from 0 to 110 n_c, with n_c the critical density which, for the 800 nm wavelength considered here, equals to $n_c \approx 1.74 \times 10^{21}$ cm^{-3}, in 2 μm so as to model the preplasma which is expected to be created by the laser prepulse. Then, the plasma density is constant for a length which is equal to the target thickness plus the contaminant layer thickness, and finally abrouptly falls to zero in a step-like fashion.

In both the preplasma and in the target region the electrons are locally neutralized by a fully ionized ($Z = 22, A = 48$), Ti background of density equal to five times the critical density. Furthermore, in the contaminant layer the electrons are locally neutralized by a proton background ($Z = 1$, $A = 1$) of density equal to that of the negatively charged particles. The laser is assumed to be gaussian in time with a 70 fs pulse duration FWHM (Full Width at Half Maximum) and with a peak intensity of 5×10^{19} W/cm^2, and it impinges normally on the target side on which the plasma presents the density ramp, i.e. from left to right when referring to Figure 8.

In the model simulations the thickness of the Ti foil and of the contaminant layer were 5 μm and 20 nm, respectively. The quantity we were particularly interested in was the energy range of the forward emitted protons, which could provide a reference value for comparison with the above experimental results. In order to ensure sufficient statistical confidence to such a numerically obtained quantity we define the numerical max proton energy as the energy $U_{\rm p,M}$ such that 95 % of the protons in the simulation acquire an energy less than $U_{\rm p,M}$.

According to our PIC simulations, we find that, $U_{\rm p,M} \approx 4.4$ MeV, which is therefore consistent with the above reported experimental value of 3.56 MeV. In a similar way, we find that the maximum energy of the Ti ions we obtain

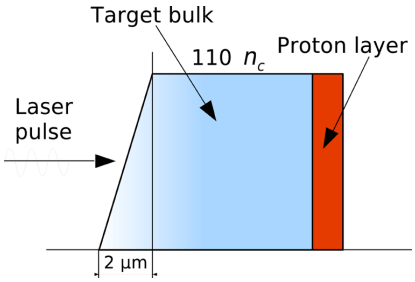

FIG. 8: Schematic diagram showing the main features of the electron density profile used in the PIC simulations.

from the simulations is $U_{\mathrm{i,M}} \approx 60$ MeV. According to the numerical code SRIM the stopping range of 60 MeV ions in alluminium is roughly equal to 13 μm, which is definitely smaller than the thickness of the Al foil used in our experiment. Therefore, we can be confident that the heavy particle signal observed on the RCF was not due to Ti ions. More accurate modelling with a fully 3D code run of a more realistic target is in progress to obtain a more realistic simulation of our experiment.

V. CONCLUSIONS

Proton production in the energy range between 1 MeV and 3.5 MeV and with a beam half-angle divergence of 10° has been achieved by irradiation of multi-layer targets of different thickness and material using a table-top, 70 fs, 600 mJ Ti:Sa laser. Both the type and the energy range and of the detected charged particles have been identified by comparison of experimental data with preliminary numerical, PIC simulations. In addition, our results strongly suggest that rear target coating with a proton rich material like lacquer significantly increases the proton yield and enables a control of the uniformity and collimation of the proton beam, even in a small scale laboratory environment, making it possible to conceive compact proton sources from a fully optical energy driver.

Acknowledgments

We acknowledge financial support by the two MIUR-FIRB projects "SPARX" (Sorgente Pulsata Auto-amplificata di Radiazione X) and "BLISS" (Broadband Laser for ICF Strategic Studies). We also acknowledge the MIUR-FSRIS project "Impianti Innovativi multiscopo per la produzione di radiazione X" and by the INFN project PLASMON-X. Access to the IOQ installation was supported by LASERLAB. We thank J.R. Cary for the use of the VORPAL code for the preliminary modeling of the data. We also wish to acknowledge the ENEA-GRID parallel computer initiative at the Laboratori Nazionali di Frascati, Italy for the execution of the numerical code calculations. The work described in this report is part of the "High Field Photonics" CNR Research Unit.

---

* also at INFN, Sezione di Pisa, Largo B. Pontecorvo 3, Pisa, Italy; also at Dip. Fisica, Università di Pisa, Italy; also at Accademia Navale, Livorno, Italy
† also at INFN, Laboratori Nazionaii di Frascati, Italy
‡ also at INFN, Sezione di Pisa, Largo B. Pontecorvo 3, Pisa, Italy
§ also at INFN, Sezione di Pisa, Largo B. Pontecorvo 3, Pisa, Italy; also at Dip. Fisica, Università di Pisa, Italy
¶ also at INFN, Sezione di Pisa, Largo B. Pontecorvo 3, Pisa, Italy; Electronic address: la.gizzi@ipcf.cnr.it

[1] G. Mourou *et al.*, Rev. Mod. Phys. **78** (2006).
[2] K. Krushelnick, Phys. Plasmas **7**, 2055 (2000).
[3] S. P. Hatchett *et al.*, Phys. Plasmas **7**, 2076 (2000).
[4] R. A. Snavely *et al.*, Phys. Rev. Lett. **85**, 2945 (2000).
[5] H. Habara *et al.*, Phys. Rev. E **69**, 036407 (2004).
[6] P. McKenna *et al.*, Phys. Rev. E **70**, 036405 (2004).
[7] M. Borghesi *et al.*, Phys. Plasmas **9**, 2214 (2002).
[8] L. Romagnani *et al.*, Phys. Rev. Lett. **95** 195001, (2005).
[9] F. Cornolti *et al.*, Phys.Rev. E **71**, 056407 (2005).
[10] A. J. Mackinnon *et al.*, Phys. Rev. Lett. **97** 045001, (2006).

[11] M. Kaluza *et al.*, Phys. Rev. Lett. **93**, 045003 (2004).
[12] T. Ceccotti *et al.*, Phys. Rev. Lett. **99**, 185002 (2007).
[13] S.V. Bulanov *et al.* Phys. Lett. A **299**, 240 (2002).
[14] S.V. Bulanov and V. S. Khoroshkov, Plasma. Phys. Rep. **28**, 453 (2002).
[15] T. Zh. Esirkepov *et al.*, Phys. Rev Lett. **89**, 175003 (2002).
[16] R. Orecchia *et al.*, Critical Reviews in Oncology/Hemathology **51**, 81 (2004).
[17] A. Brahme, Int. J. Radiat. Oncol. Biol. Phys. **58**, 603 (2004).
[18] W. K. Weyrather and J. Debus, Clinical Oncology **15**, s23 (2003).
[19] H. Tsujii, Eur. J. Cancer **37**, s251 (2004).
[20] R. Orecchia *et al.*, Eur. J. Cancer **34**, 459 (1998).
[21] U. Amaldi, Analysis **1**, 1 (2003).
[22] S. Atzeni and J. Meyer-ter-vehn, *The physics of inertial confinement fusion, beam plasma interaction, hydrodynamics, hot dense matter*, Clarendon press, Oxford (2004).
[23] M. Roth *et al.*, Phys. Rev. Lett. **86**, 436 (2001).
[24] M. Borghesi *et al.*, Phys. Plasmas **9**, 2214 (2002).
[25] M. Borghesi *et al.*, Phys. Rev. Lett. **92**, 055003 (2004).
[26] F. Califano, F. Pegoraro and S. V. Bulanov, Phys. Rev. E **68**, 066406 (2003).
[27] M. Borghesi *et al.*, Phys. Rev. Lett. **88**, 135002 (2004).
[28] T. E. Cowan *et al.*, Phys. Rev. Lett. **92**, 204801 (2004).
[29] A. J. Kemp *et al.*, Phys. Rev. E **75**, 056401 (2007).
[30] S. J. Gitomer *et al.*, Phys. Fluids **29** 2679 (1986).
[31] M. Allen *et al.*, Phys, ReV. Lett. **93** 265004 (2004).
[32] S. Betti, F. Ceccherini, F. Cornolti and F. Pegoraro, Plasma Phys. Contr. Fusion **47**, 521-529 (2005).
[33] F. Ceccherini, S. Betti, F. Cornolti and F. Pegoraro, Laser Phys. **16**, 594-599 (2006).
[34] P. Mora, Phys. Rev. E **72**, 056401 (2005).
[35] J. Fuchs *et al.* Nature Physics **2**, 48 (2006).
[36] L.A. Gizzi *et al.*, Plasma Phys. Contr. Fus. **49**, B211-B221 (2007).
[37] E. Breschi *et al.*, Nucl. Instr. Meth. A **522**, 190 (2004) and references therein.
[38] L. Romagnani *et al.*, Phys. Rev. Lett. **95**, 195001 (2005).
[39] M. Borghesi *et al.*, Phys. Rev. Lett. **92**, 055003 (2004).
[40] Freely downloadable online at `http://www.srim.org`.
[41] C. Nieter and J. Cary, J. Comput. Phys. **196** 448 (2004).